AECL EACL

AECL CANDU EACL CANDU

INTEGRITY: A Semi-Mechanistic Model for Stress Corrosion Cracking of Fuel

IAEA Technical Committee Meeting on Water Reactor Fuel Element Modelling at High Burnup and its Experimental Support

Windermere, United Kingdom

AECL-10792

by M. Tayal*, K. Hallgrimson*, J. MacQuarrie*, P. Alavi*, S. Sato*, Y. Kinoshita** and T. Nishimura**

* AECL, Mississauga, Ontario, Canada
** Electric Power Development Company Limited Toyko, Japan

1994 Sept. 19-23 19-23 Sept, 1994

AECL CANDU
2251 Speakman Drive
Mississauga, Ontario
Canada L5K 1B2

EACL CANDU
2251, rue Speakman
Mississauga (Ontario)
Canada L5K 1B2

942218/450
Tayal
94/09/07

942218/450
Tayal
94/09/22

AECL EACL

AECL CANDU EACL CANDU

INTEGRITY: A Semi-Mechanistic Model for Stress Corrosion Cracking of Fuel

IAEA Technical Committee Meeting on Water Reactor Fuel Element Modelling at High Burnup and its Experimental Support

Windermere, United Kingdom

AECL-10792

by M. Tayal, K. Hallgrimson, J. MacQuarrie, P. Alavi, S. Sato, Y. Kinoshita and T. Nishimura

Abstract

In this paper we describe the features, validation, and illustrative applications of a semi-mechanistic model, INTEGRITY, which calculates the probability of fuel defects due to stress corrosion cracking. The model expresses the defect probability in terms of fundamental parameters such as local stresses, local strains, and fission product concentration. The assessments of defect probability continue to reflect the influences of conventional parameters like ramped power, power-ramp, burnup and Canlub coating. In addition, the INTEGRITY model provides a mechanism to account for the impacts of additional factors involving detailed fuel design and reactor operation. Some examples of the latter include pellet density, pellet shape and size, sheath diameter and thickness, pellet/sheath clearance, coolant temperature and pressure, etc. The model has been fitted to a database of 554 power-ramp irradiations of CANDU fuel with and without Canlub. For this database the INTEGRITY model calculates 75 defects versus 75 actual defects. Similarly good agreements were noted in the different sub-groups of the data involving non-Canlub, thin-Canlub, and thick-Canlub fuel. Moreover, the shapes and the locations of the defect thresholds were consistent with all the above defects as well as with additional 14 ripple defects that were not in the above database. Two illustrative examples demonstrate how the defect thresholds are influenced by changes in the internal design of the fuel element and by extended burnup.

1993 Sept. 19-23

19-23 Sept. 1993

AECL CANDU
2251 Speakman Drive
Mississauga, Ontario
Canada L5K 1B2

EACL CANDU
2251, rue Speakman
Mississauga (Ontario)
Canada L5K 1B2

942218/450
Tayal
94/09/07

AECL EACL

AECL CANDU EACL CANDU

INTEGRITY: Modèle semi-mécaniste de la fissuration par corrosion sous contrainte du combustible

Réunion du Comité technique de l'AIEA sur la modélisation de l'élément combustible du réacteur à eau aux fortes combustions et les expériences à l'appui.

Windermere, Royaume-Uni

AECL-10792

par M. Tayal, K. Hallgrimson, J. MacQuarrie, P. Alavi, S. Sato, Y. Kinoshita et T. Nishimura

Résumé

Le présent ouvrage décrit les caractéristiques, la validation et les applications typiques d'un modèle semi-mécaniste appelé «INTEGRITY» qui calcule la probabilité des ruptures de gaine causées par la fissuration par corrosion sous contrainte. Le modèle exprime cette probabilité par des paramètres fondamentaux, par exemple les contraintes locales, la déformation locale et la concentration de produits de fission. Les calculs de probabilité de défaillance (rupture de gaine) tiennent toujours compte des paramètres classiques commes les variations de la puissance par rampes, les rampes de puissance, la combustion massique et l'enrobage Canlub. De plus, le modèle INTEGRITY prend en compte dans ses calculs d'autres facteurs touchant par exemple l'étude détaillée du combustible et le fonctionnement du réacteur. Parmi ces derniers facteurs, on retrouve la densité de la pastille, la forme et la taille de la pastille, le diamètre et l'épaisseur de la gaine, le jeu entre les pastilles et la gaine, la température et la pression du caloporteur, etc. Le modèle utilise une base de données contenant les données de 554 irradiations du combustible CANDU avec et sans enrobage Canlub, dans des conditions de variation continue de la puissance. Utilisant cette base de données, le modèle a calculé 75 défaillances théoriques contre 75 défaillances réelles. Des résultats tout aussi bons ont été obtenus dans les différents sous-groupes de données liés à l'absence d'enrobage Canlub, à une mince couche de Canlub et à une épaisse couche de Canlub. Par ailleurs, la forme et l'emplacement des seuils de défaillance étaient exacts pour toutes les défaillances susmentionnées ainsi que pour 14 autres défaillances secondaires qui ne figuraient pas dans la base de données. On donne deux exemples pour illustrer comment les modifications apportées à la structure interne de l'élément combustible et comment les fortes combustions influent sur les seuils de défaillance.

1993 Sept. 19-23 Du 19 au 23 sept. [illegible]

AECL CANDU
2251 Speakman Drive
Mississauga, Ontario
Canada L5K 1B2

EACL CANDU
2251, rue Speakman
Mississauga (Ontario)
Canada L5K 1B2

942218/450
Tayal
94/09/07

TABLE OF CONTENTS

TABLE OF CONTENTS

SECTION **PAGE**

List of Figures

1. INTRODUCTION

The performance record of CANDU* fuel is excellent, with fuel bundle integrity exceeding 99.9% [1]. Most of the defects occurred during identifiable departures from the norm, and helped improve our understanding of the nature and level of defect probabilities. Previous surveys of the defects have shown that in these small number of defects, stress corrosion cracking (SCC) is an important mechanism for fuel failures [1].

At present empirical correlations [2, 3, 4] are available to define the limits of powers and of power-ramps within which CANDU fuel can be operated without risk of failure from SCC under normal operating conditions. Their use is generally recommended within the ranges of their respective databases. Often fuel engineers also need to assess the impact of operating fuel under conditions beyond the existing database, for example: extended burnups; mixed oxide (MOX) fuel; slightly enriched (SEU) fuel; manufacturing variations/flaws; variations in pellet density; diametral/axial clearances; pellet length and shape; element diameter; etc. These applications generally fall outside the range of the existing databases of the empirical correlations. To help assess the likelihood of SCC under such conditions, a semi-mechanistic approach for SCC, called INTEGRITY [5], was developed in 1990.

This paper presents an evolution of the above concept and contains improved equations that increase the accuracy of the INTEGRITY model. The improved model – called INTEGRITY-2 – has been based on and compared to a database of 554 power-ramp irradiations and 14 ripple defects of CANDU fuel. The results are presented here.

At this time the applicability of INTEGRITY-2 is limited to stress corrosion cracking at circumferential ridges due to single power-ramps with dwell periods of 2.5 h or longer.

In this paper we first provide some technical background relevant to SCC, followed by a discussion of the mechanistic equations and their validation. Two illustrative examples show how the defect thresholds are influenced by changes in the internal deign of the fuel element and by extended burnup.

Figure 1 defines some of the terms used in this paper. The nomenclature is given towards the end.

2. BACKGROUND

SCC of fuel element cladding occurs when the irradiation-embrittled sheath experiences high tensile stresses/strains in the presence of a corrosive internal environment provided by the fission products. It may also be influenced by hydrides, which can provide sites for crack initiation and which can also blunt the growth of cracks [6, 7].

---

* CANDU: CANada Deuterium Uranium

The high tensile stresses occur mostly due to pellet expansion because of power-ramps. These result from on-power fuelling and/or from changes in reactor power. Tensile stresses can also potentially be caused by excessive pressure of fission gas. Thus SCC assessments are important because collapsible sheaths experience higher stresses/strains, and because the comparatively higher operating powers of CANDU fuel lead to higher fission gas release.

About 80-90% of the defects during SCC-excursions so far in commercial CANDU reactors have occurred at circumferential ridges and were caused by power-ramps. Therefore the focus of this paper is on SCC defects at circumferential ridges caused by power-ramps.

Most of the remaining SCC defects have occurred at the re-entrant corner near the sheath/endcap weld, and were also caused by power-ramps. A few isolated SCC defects have also occurred due to excessive gas pressures at high burnups. At a later date we expect to expand INTEGRITY-2 to also cover the latter two subsets of SCC defects.

Both the locations noted above (circumferential ridge, endcap weld) are locations of stress/strain concentrations.

Many factors contribute to SCC in CANDU fuel. There is convincing evidence [6, 7, 8] that the likelihood of SCC is influenced by the following factors: the local tensile stresses and strains; the local concentration of corrodants at the crack tip; the duration of tensile stresses/strains; and the influences of microstructure, of hydrides and of irradiation on the resistance of Zircaloy to SCC. The studies to-date have focused on iodine, on cesium, and on cadmium as the likely corrodants.

We call these the mechanistic parameters pertinent to SCC. The mechanistic parameters, in turn, are affected by a number of operational and design parameters. For example, the effects of ramped power, of power-ramp, of burnup, of dwell time, and of Canlub have been documented extensively [2, 6, 8].

In addition, in the area of ridge stresses/strains, IRDMR* experiments have demonstrated that ridge strains are increased by higher density of UO_2, by faster ramp-rates, and by increased burnups [9]. Similarly, Carter has shown that longer pellets also increase the ridge strain[10]. A study of 1988 Pickering defects has suggested [11] that fuel containing long dense pellets is more susceptible to SCC.

Likewise, in the area of corrosive internal environment, enrichment changes the heat generation rate profile within the fuel element. This changes the pellet temperature and hence the fission gas release. Previous reviews have suggested that enriched CANDU fuel power-ramped in research reactors (NRU/NRX) is more susceptible to SCC than natural-uranium fuel ramped in commercial CANDU reactors [2]. Also, gamma-radiography has demonstrated that some fission products tend to concentrate at the interfaces between neighbouring pellets [12]. For example, Lysell and Schrire report that the concentrations of I-131, I-133, Cs-134, and Cs-137 are a factor of 4 to 14 higher at the pellet interfaces compared to the mid-pellet positions [12]. This means that the number of pellets in the stack can also affect the local concentration of corrosives.

---

* IRDMR: In-Reactor Diameter Measurement Rig

IRDMR measurements show that repeated power cycles give persistent strain cycles [13]. This can lead to a combination of SCC and corrosion-assisted fatigue [14]. Similarly, multiple ramps in power have been noted to fail fuel more easily, via the effect of unrelaxed stresses from previous ramps.

In the past, empirical correlations [2, 3, 4] have been developed to assess the likelihood of SCC failures. Two analytically-based models [5, 15] have also been developed.

The empirical correlations generally express the defect probability as a function of: power-ramp (ΔP); ramped power (P_{max}); and burnup (ω). Sometimes the effects of dwell time and of graphite thickness are also considered.

In these, the power-ramp represents the stresses and the strains in the sheath at the ridge. The combination of ramped power, burnup, and graphite thickness represents the concentration of corrosive fission products at the inner surface of the sheath. The resistance of the sheath to SCC is represented by burnup.

As noted earlier, in addition to the operational parameters such as power ramp, ramped power, and burnup that are covered explicitly in the empirical correlations, SCC is also influenced by several design parameters such as pellet density, clearances, pellet shape, etc. The INTEGRITY model is being developed to address factors like these.

3. DATA COLLECTION

A considerable database was compiled for this study, including out-reactor tests and in-reactor ramps.

3.1 OUT-REACTOR DATA

We used Lunde and Videm's out-reactor measurements [16] on irradiated Zircaloy to quantify the effect of fluence (burnup) on the threshold stress for SCC. The data covers burnups up to 800 MW.h/kgU – see Figure 2a. The figure exhibits the expected trend that for a given hold period and corrodant concentration, the threshold stress for SCC generally decreases with burnup.

Figure 2a also shows that for a given fluence (burnup), the threshold stress for SCC depends on the concentration of the corrodant at the sheath surface. With higher concentration of the corrodant, failure threshold is reached at lower stresses for any given burnup. Thus there is a threshold combination of stress and corrodant concentration for a given burnup. This means that for each burnup one can expect a series of threshold ramped powers (ΔPs), each corresponding to a different maximum power (P_{max}). This is illustrated further in the next section.

3.2 IN-REACTOR DATA

We also compiled a database of 568 power-increases involving 89 SCC defects at circumferential ridges under conditions of long dwell periods. They cover information from CANDU power reactors as well as from research reactors (NRU/NRX).

The data covers the following ranges:

- Ramped powers: 28 to 92 kW/m
- Power ramps: 6 to 60 kW/m
- Burnups: up to 742 MWh/kgU

The above data can be divided into the following four categories:

- Non-Canlub Ramps: 50 defects in 410 ramps;
- Non-Canlub Ripples: 14 defects. No information is readily available for intact fuel in this category;
- Thin-Canlub Ramps: 8 defects in 21 ramps;
- Thick-Canlub Ramps: 17 defects in 123 ramps.

Thus the defect probability can be calculated for the ramp data, providing a total of 75 defects in 554 irradiations. The ripple data provides 14 additional irradiations which can help locate defect thresholds but do not quantify defect probabilities.

We checked if the ramp and ripple defects come from the same population. For this purpose, we reviewed the non-Canlub defects that are close to the defect thresholds. The results are shown in Figures 2b to 2d. The ramp and ripple thresholds seem to form separate populations for maximum power as well as for power-increase – see Figures 2b and 2c.

Compared to the ramps, the ripples are generally associated with higher maximum power (Figure 2b) and lower power-ramps (Figure 2c). This can be related to the generally higher initial powers involved in the ripple data. This is further illustrated in Figure 2d, which shows idealized power histories for typical ramp and ripple defects at ~220 MW.h/kgU. It is clear that the ripple defects operated at initial powers higher than the maximum power threshold for the ramp defects. Thus they had higher amounts of fission products and required comparatively small power-ramps for the defects.

This is similar to the effect of iodine noted earlier from the independent data of Lunde and Videm [16] – see Figure 2a – where higher amount of iodine lowered the threshold stress for SCC.

From this we conclude that the thresholds for maximum power and for power-ramp are mutually dependent on each other.

We note that at this time the defect data is available in terms of bundle defects for 89 ramps/568 irradiations, and in terms of element defects for only 39 ramps/158 irradiations. Our mechanistic model uses the bundle-defect data so that the model can benefit from the much larger database.

4. DEFINITIONS OF MECHANISTIC TERMS

Following Reference 5, we based our mechanistic model on fission product concentration, work density, and SCC-resistance. In this section we give their definitions.

The fission product concentration, f, represents the corrodant concentration at the inside surface of the sheath at the ridge.

The work density, u, is the area under the stress-strain curve. It is calculated by using the following equation:

$$u = \int \sigma_{11}\, d\varepsilon_{11} + \int \sigma_{22}\, d\varepsilon_{22} + \int \sigma_{33}\, d\varepsilon_{33} + \int \sigma_{13}\, d\varepsilon_{13}$$

where the integral is taken over the power-ramp. The symbols "σ" and "ε" represent the local stresses and strains respectively, and the subscripts 1, 2, 3 represent the radial, circumferential, and axial directions respectively. Thus the work density represents the combined influences of the radial, hoop, axial, and shear components of the elastic-plastic stresses and strains. It is equal to the work done, or energy imparted to the sheath by the expanding pellet.

The SCC-resistance measures Zircaloy's inherent resistance to failure via SCC. We define it as the work density required to fail Zircaloy via SCC at a given burnup and fission product concentration.

The mathematical details of the model are given in the next section.

5. MATHEMATICAL FORMULATIONS

a. The shape of the curve for SCC-resistance was derived from the out-reactor data of Lunde and Videm [16]. As noted earlier, the above data is valid up to 800 MW.h/kgU. The equation of this shape is given by:

$$u_s = 2.358 \times 10^{12}\, F^{-0.6056} \qquad (1)$$

where

$$F = 7.58 \times 10^{18} \omega \qquad (2)$$

b. Next, we calculated the work densities for the 568 power increases described in the previous section. This was done by using the ELESTRES code [17] to calculate the incremental pellet displacements during the ramp, and the FEAST code [18] to calculate the resulting stresses, strains, and work densities at the inner surface of the sheath at the ridge. The FEAST calculations considered elastic-plastic effects. To account for the effects of local stress/strain concentrations at the circumferential ridge, a graded mesh of about 300 axisymmetric finite elements was used [17]. The SHEATH code was used to automate the calculations. Thus the work density reflects the influences of parameters like the size of the power-ramp, pellet density, diametral clearance, pellet shape (e.g. length, chamfer size, land width, dish depth), coolant pressure, etc., on the stresses and strains in the sheath.

c. The above work density was expressed in non-dimensional form by defining the work density ratio (W) as follows:

$$W = u/u_s \qquad (3)$$

Thus the work density ratio incorporates the shape of threshold stresses measured by Lunde and Videm.

d. Then we used ELESTRES to calculate the fission gas released to the pellet-sheath gap. For this calculation, we used a dwell time of 2.5 h [2] and calculated the average fission gas in the gap during the above hold after the ramp.

This was converted to fission product factor in the gap as follows – please see the nomenclature given at the end:

$$g = \frac{VD}{2\,\pi\, rl\,(n+1)} \qquad (4)$$

The above equation reflects the experimental evidence on I-131 noted earlier, in that it allows the corrosive fraction of the fission products to concentrate in narrow rings at inter-pellet interfaces. The fission product factor in the gap, g, is a function of the operating conditions and fuel design. It covers the combined influences of parameters such as ramped power, burnup, sheath diameter, number of pellets, pellet density, initial power and coolant temperature, on the the amount of fission products at the inner surface of the sheath.

e. We next calculated the fission product concentration at the inside surface of the sheath at the ridge, f. To do this we subtracted the protection provided by Canlub, c, from the fission product concentration in the gap, g:

$$f = g\text{-}c \qquad (5)$$

In equation (5) the net effect of Canlub is considered equivalent to a net reduction in the amount of fission products that reach the surface of the sheath.

f. The protection provided by Canlub, c, was considered proportional to the mass of Canlub for high values of fission product release. At low values of fission product release, the protection was considered to also depend on the concentration of the fission gas in the gap. Thus, based on a statistical analysis, 'c' was defined as follows:

$$c = \text{minimum of } \{g, \text{ or } [1 - \exp(-\sqrt{(qm)})]\, g, \text{ or } vm\} \qquad (6)$$

Here, "m" is the mass of graphite at the ridge and is calculated from:

$$m = 2\pi rlt\,\rho \qquad (7)$$

Thus thicker Canlub is considered to provide greater protection against SCC. In INTEGRITY the effect of Canlub is treated as a continuous function of graphite thickness rather than a series of separate curves for no-, thin-, or thick-Canlub.

g. A "Damage Index" d was defined to assess the combined influences of the work density ratio and the fission product concentration as follows:

$$d = aW^x f^y \tag{8}$$

This form of the damage index ensures that zero damage is assigned if either the work density or the fission product concentration is zero.

h. From this, a defect probability "p" was defined as [3, 4]:

$$p = \frac{1}{1 + \exp\{-(d - z)\}} \tag{9}$$

i. The six empirical coefficients, a, q, v, x, y and z, were found by a least-squares regression analysis to fit the actual number of defects observed in the previous database. The methodology outlined by R. daSilva was used [4]. Four of the coefficients, a, x, y, and z, define the influences of work density ratio and of fission product concentration on the defect probability. For these trends the most reliable statistical guidance is provided by the non-Canlub ramp data because it is the most numerous. Hence this data was given the highest weight in determining these four coefficients. The thick-Canlub data was used mainly to quantify the effect of Canlub, viz. coefficients q and m. The thin-Canlub data was not used to obtain the coefficients because it contains only 21 irradiations, hence it was considered too small for statistical purposes. The non-Canlub ripple data was also not used because for that set we do not have data on intact fuel at this time, hence the defect probabilities cannot be quantified for them. Nevertheless, the final correlation was tested for consistency against all four sets of data.

In obtaining the least squares fit, we set the defect probability to 1% [2] for the non-Canlub ramp defect with the lowest value of the damage parameter.

6. GOODNESS OF FIT

The goodness of fit was checked by six separate methods: a) Number of observed versus calculated defects; b) Shapes of calculated defect thresholds versus data; c) Distribution of defects in risk groups; d) Distribution of defects on the basis of defect probability; e) Distribution of defect probability; and f) Discrimination of defects/intacts. These are described in the following paragraphs.

a. Number of Observed versus Calculated Defects

We used the model to calculate the expected number of defects in the 3 sets of data for which the defect/intact statistics are available (i.e., excluding non-Canlub ripples). The following results were obtained: In the 410 non-Canlub ramps, the model calculated 50 defects vs. the actual number of 50. In the 21 thin-Canlub ramps, the model calculated 8 defects vsersus the actual 8. In the 123 thick-Canlub ramps, the model calculated 17 defects versus the actual 17. Thus in all, for the 554 ramps, the model calculated a total of 75 defects which is the same as the actual number (also 75).

The above information is displayed in Figure 3. The calculated numbers match the observed defects well.

b. Shapes of Calculated Defect Thresholds versus Data

Figures 4a and 4b show typical shapes of calculated defect thresholds vs data. Note from Figure 4a that the calculated shape of the ΔP threshold changes its curvature sharply at ~100 MW.h/KgU. This is very similar to the actual data. Figure 4b shows that the calculated thresholds for the non-Canlub ripple defects are consistent with the actual data, even though this data was not used in the derivation of the coefficients.

c. Distribution of Defects in Risk Groups

This comparison follows the suggestions made by R. daSilva in Reference 14. Accordingly, the data were arranged in ascending order (smallest to highest) of the damage index. They were then split into ten groups, each containing similar number of ramps, to form deciles of risk tables. For each decile, the calculated number of defects were compared to the actual defects. Typical results are shown in Figure 4c. The trends of the calculations generally agree well with the observations.

d. Distribution of Defects on the Basis of Defect Probability

This is an alternate method of examining the detailed distribution of defect probabilities, and can be used for correlations which do not explicitly quantify the risk below the defect threshold (e.g. Fuelograms [2]). Although our model does define a damage index, we are nevertheless providing this additional information for comparison and for consistency with past results. In this method, the data is grouped into ten sets depending on the calculated defect probability, for example defect probability of 0-10%, 10-20%, etc. For each set, the actual defect probability is compared with the calculated. Typical results are shown in Figure 4d. The two numbers beside each point in Figure 4d specify the number of actual defects and the total number of irradiations in that set, respectively. For example, the set representing 0-10% calculated defect probability contains 20 actual defects in 314 irradiations. The comparison is tenuous in regions where the statistics are small. Overall, our model is in reasonable agreement with data.

e. Distribution of Defect Probability

Figure 5 shows how the defect probability is influenced by the damage index for all four sets of data. The expected s-shaped curve is clearly visible. Also, if the model were good, the density of defects should get progressively higher with increasing damage index. This is indeed exhibited by the data. Further, for the model to be good, all the defects should have a calculated defect probability of 1% or higher. This too is exhibited by the data, including the ripple defects.

f. Discrimination of Defects/Intacts

Figure 6 checks how well the defect thresholds mark the onset of failures for all four sets of data (i.e. including the non-Canlub ripple defects). All the actual defects lie above the calculated 1% defect threshold, indicating that the calculated thresholds are consistent with the actual data.

In Figure 6, the non-Canlub ripple defects generally lie at the highest fission product concentrations. This reflects their comparatively high pre-ramp powers.

Canlub prevents some of the fission gas in the gap from reaching the sheath surface. Thus the Canlub failures occur for lower values of fission product concentration and correspondingly higher values of work density ratio. This effect is more pronounced in thick Canlub fuel, and is also visible in Figure 6.

7. FEATURES OF THE MODEL

- The shape of the defect threshold is based on out-reactor tests which define a basic, continuously-varying material property (SCC threshold). Hence the accuracy of the shape is not subject to the comparatively larger uncertainty expected in defect thresholds derived solely from a limited number of yes/no type of in-reactor defects. Thus the model is usable in the range of the database of the above out-reactor tests.

- Although the shapes of the defect thresholds are derived from out-reactor data, they do match quite well with the available in-reactor data on 568 power-increases. Also, the calculated number and distribution of defects agree well with the actual data.

- One set of equations correlates well with four different sets of data, i.e., non-Canlub ramps; non-Canlub ripples; thin-Canlub ramps; and thick-Canlub ramps. This provides confidence that the pertinent trends are captured well.

- The defect probability curves show continuous variations with operational parameters like ΔP and P_{max}. Thus some of the unnatural jumps and plateaus exhibited by a previous empirical correlation have been eliminated.

- The principles of statistics are followed rigorously. This has eliminated a weakness of a previous empirical correlation.

- The model recognizes the interdependence of P_{max} and ΔP in determining the defect thresholds. This makes it consistent with the observed differences in ramp and ripple defect thresholds, as well as with the differences in stress thresholds observed by Lunde and Videm for different corrodant concentrations.

- The model incorporates the influence of operational parameters such as power-ramps, ramped powers, coolant temperature, and coolant pressure; and of design variables such as Canlub mass, pellet density, clearances and pellet shape, etc.

- The model is considered valid for burnups up to 800 MW.h/kgU; infinite dwell times (longer than 2.5 h); and single ramps in power. The model is limited to estimates of defect probability due to stress corrosion cracking at circumferential ridges.

The next two sections provide illustrative examples on the use of the INTEGRITY model.

8. ILLUSTRATIVE EXAMPLE #1: PELLET DENSITY

As an illustrative example, we assessed the influence of pellet density on the defect probability of 37-element CANDU fuel. Figure 7a shows the power history considered, consisting of a ramp of 35 kW/m to a maximum power of 56 kW/m at 100 MW.h/kgU. Figure 7b shows the calculated trends of the damage index, and demonstrate the opposing effects of density, pellet temperature and porosity. At low densities, increasing the density decreases pellet temperatures which decreases the damage index. At higher densities, the low porosity in high-density fuel causes higher expansion of the pellet, which increases the damage index. For this power history the defect probability stays below 1% for pellet densities less than 10.8 g/cc.

9. ILLUSTRATIVE EXAMPLE #2: HIGH BURNUP

As another illustrative example, we assessed the influence of extended burnup – about 700 MW.h/kgU – on the integrity of a fuel element of reduced diameter containing slightly enriched uranium fuel. An optimized pellet shape was considered featuring short pellets, big chamfers, big land, and reduced density [19]. Figure 7c shows the combinations of power-ramps/ramped-powers considered. The ramped powers range from 25 to 56 kW/m, and the power-ramps from 1 to 40 kW/m. Figure 7d shows the calculated damage index. Again, the calculated trends look reasonable. The defect probabilities reflect a balance between higher fission gas release due to enrichment, lower volume of fission gas release due to smaller diameter, tendency for higher concentration of fission products due to reduced diameter, and lower stresses/strains due to the optimized shape and density of the pellet.

10. DISCUSSION

The INTEGRITY model discussed here does not replace the empirical correlations now in use. Rather, it provides a means of extending the range of applicability of the correlations, to conditions that are either not covered by the existing data base or are sparsely represented.

The INTEGRITY model continues to reflect the influences of operational parameters that are currently used in existing empirical correlations for defect thresholds/probabilities, viz: power-ramp, ramped power, and burnup. In addition, it provides a vehicle to account for the impacts of detailed fuel design parameters such as pellet density, pellet shape and size, sheath diameter and thickness, pellet/sheath clearances, etc. Additional operational parameters can also be covered, for example coolant temperature and pressure, etc. As noted earlier, previous experiments and irradiations have already demonstrated that combinations of the above features can have considerable impacts on factors such as stresses, strains, and fission gas releases, and hence on SCC defects.

The examples discussed above demonstrate how INTEGRITY can be applied to obtain first-order estimates of defect thresholds and probabilities in situations where sufficient empirical data may not exist to provide reliable guidance. With further evolution, some specific applications of the preceding concepts could include the following:

10.1 GUIDE THE ACCEPTANCE/LOADING OF NEW FUEL

Sometimes the as-fabricated fuel contains combinations of tolerances that are not sufficiently covered by the previous well-characterized database on ramp testing. One example is fuel of high mass, including high UO_2 density and low clearances. Or, the fuel may contain manufacturing flaws whose impact is unknown from previous tests. The approach outlined here can help provide an interim guidance about the expected performance of such fuel.

10.2 AID FUEL SPECIFICATIONS

The model can be used to define the sensitivity of SCC defects for combinations of fuel fabrication parameters like pellet density, pellet shape, pellet/sheath clearances, etc. This can help confirm that the limits in fuel specifications reflect only the safe combinations of above and related parameters.

10.3 GUIDE REACTOR OPERATION

Similarly, the approach can help guide reactor operation in new areas of operation, e.g., effects of power cycles, extended burnups, non-routine startups, non-routine fuelling, etc.

10.4 AID EVOLUTION OF FUEL DESIGN

Some specific fuel evolution activities currently underway include [1]: High Burnup Fuel, Slightly Enriched Uranium Fuel, Fuel for Highly Advanced Core, Low Void Reactivity Bundle, Mixed Oxide (MOX) Fuel, and DUPIC (Direct Use of PWR Fuel in CANDU). Again, the approach outlined above can be applied in these evolutions.

11. CONCLUSIONS

a. Two independent sets of data suggest that defect thresholds for maximum power (fission products) and for power-ramp (stresses/strains) are mutually dependent on each other.

b. A mechanistic model called INTEGRITY-2 has been developed for assessing SCC at ridges. It accounts for fuel design as well as operational parameters in calculating SCC. Its applicability extends to burnups of 800 MW.h/kgU.

c. The model shows excellent fit with defect statistics in 554 ramps. In particular, checks show:

   - 50 calculated defects vs. 50 actual defects in 410 non-Canlub ramps;
   - 8 calculated versus 8 actual defects in 21 thin-Canlub ramps; and
   - 17 calculated versus 17 actual defects in 123 thick-Canlub ramps.

d. The shapes of the defect threshold curves are consistent with the distributions of the actual data noted above, and with 14 additional defects involving power ripples in non-Canlub fuel. The calculated distributions of the defects in different risk regions are also consistent with actual data.

e. The model contains a term for the mass of Canlub, so any thickness of Canlub can be assessed.

f. An illustrative example shows that the pellet density first decreases, then increases, the defect probability. This is due to the competing influences of pellet temperature and pellet porosity. Another illustrative example suggests that fuel integrity can be enhanced by optimizing the shape and density of the pellet.

12. ACKNOWLEDGEMENTS

We thank Mr. T. Tanaka (EPDC), J.W. Love (AECL), R. Sejnoha (AECL), I.E. Oldaker (AECL), T. Carter (AECL), M. Floyd (AECL), P. Chan (AECL), W. Richmond (AECL), D.E. Teed (GEC), M. Hoare (Zircatec), and J. Lawless (Univ. of Waterloo), for valuable technical discussions and help during this project. We also thank L. Lunde (Norway), K. Videm (Norway) and Journal of Nuclear Materials for permission to reproduce Figure 2a. Financial support by Electric Power Development Company Limited, Japan, is also gratefully acknowledged.

13. LIST OF SYMBOLS

a	empirical coefficient
c	empirical coefficient for the effect of Canlub on fission product concentration
d	damage index
D	density of free gas
f	fission product concentration at the sheath inner surface at the ridge ($\mu g/mm^2$)
F	fast neutron fluence (> 1 Mev) (n/cm^2)
g	fission product factor in the gap ($\mu g/mm^2$)
l	width of the ring over which the fission products concentrate at the circumferential ridge (mm)
m	mass of Canlub (μg)
n	number of pellets in the fuel element
ΔP	power-ramp (kW/m)
P_{max}	ramped power (kW/m)
p	defect probability (fraction)
q	empirical coefficient
r	inner radius of the sheath (mm)
t	thickness of Canlub (μm)

u work density (MPa)

v empirical coefficient

V volume of released fission gas

W work density ratio

x, y, z empirical coefficients

Greek Symbols

ε strain

ρ density of Canlub

σ stress

ω burnup (MW.h/kgU)

Subscript

s shape of threshold

14. REFERENCES

1. M. Gacesa, P.G. Boczar, J.H.K. Lau, P.T. Truant, N. Macici, E.G. Young, "Canadian Fuel Development Program", Third International Conference on CANDU Fuel, Canadian Nuclear Society, Pembroke, Canada, 1992 October 04-08.

2. W.J. Penn, R.K. Lo, and J.C. Wood, "CANDU Fuel – Power Ramp Performance Criteria", Nuclear Technology, 34 (1977), pp. 249-268.

3. A.J. Hains, R.L. daSilva and P.T. Truant, "Ontario Hydro Fuel Performance Experience and Development Program", International Conference on CANDU Fuel, Canadian Nuclear Society, Chalk River, 1986 October 06-08.

4. R.L. daSilva, "CAFE - A Probabilistic Model for Predicting CANDU Fuel SCC Power Ramp Failures", Third International Conference on CANDU Fuel, Pembroke, Canadian Nuclear Society, 1992 October 04-08.

5. M. Tayal, E. Millen, R. Sejnoha, G. Valli, "A Semi-Mechanistic Approach to Calculate the Probability of Fuel Defects", AECL Report AECL-10642, 1992 October.

6. B. Cox, "Pellet Clad Interaction (PCI) Failures of Zirconium Alloy Fuel Cladding - A Review", Journal of Nuclear Materials, 1990 August, Vol. 172, Issue -3, pp. 249-292.

7. B. Cox, "Environmentally Induced Cracking of Zirconium Alloys – A Review", Journal of Nuclear Materials, 1990 January, Vol. 170, Issue -1, p 1-23.

8. B. Cox, J.C. Wood, "Iodine Induced Cracking of Zircaloy Fuel Cladding – A Review", Atomic Energy of Canada Limited, Report AECL-4936, 1974.

9. P.J. Fehrenbach, P.A. Morel, R.D. Sage, "In-Reactor Measurement of Cladding Strain: Fuel Density and Relocation Effects", Nuclear Technology, Volume 56, 1982, pp. 112-119.

10. T.J. Carter, "Experimental Investigation of Various Pellet Geometries to Reduce Strains in Zirconium Alloy Cladding", Nuclear Technology, Volume 45, 1979, pp. 166-176.

11. M.R. Floyd, R.J. Chenier, D.A. Leach, R.R. Elder, "An Overview of the Examination of Fuel as a Follow-up to the 1988 November Overpower Transient in Pickering NGS-A Unit 1", Third International Conference on CANDU Fuel, Canadian Nuclear Society, Pembroke, Canada, 1992 October 04-08.

12. G. Lysell, D. Schrire, "Fission Product Distribution at Different Power Levels", IAEA Meeting on Fuel Performance at High Burnup for Water Reactors, Studsvik, Sweden, 1990 June 05-08, IWGFPT/36, pp. 132-139.

13. P.J. Fehrenbach, P.A. Morel, "In-Reactor Measurement of Clad Strain: Effect of Power History", AECL Report AECL-6686, 1980.

14. M. Tayal, A.M. Manzer, R. Sejnoha, Y. Kinoshita, A.J. Hains, "The Integrity of CANDU Fuel during Load Following", AECL Report AECL-9797, 1989.

15. M.J.F. Notley, "PRAMP – A Model for Calculating the Probability of Fuel Defects", Third International Conference on CANDU Fuel, Canadian Nuclear Society, Chalk River, Canada, 1992 October 4-8, pp 5-11 to 5-20.

16. L. Lunde, K. Videm, "The Influence of Testing Conditions and Irradiation on the Stress Corrosion Cracking Susceptibility of Zircaloy", Journal of Nuclear Materials, 95 (1980), pp. 210-218.

17. M. Tayal, "Modelling CANDU Fuel Under Normal Operating Conditions: ELESTRES Code Description", Atomic Energy of Canada Limited, Report AECL-9331, 1987.

18. M. Tayal, "FEAST: A Two-Dimensional Non-Linear Finite Element Code for Calculating Stresses", Seventh Annual Conference, Canadian Nuclear Society, 1986. Also Report AECL-8763.

19. M. Tayal, A. Ranger, P.N. Singh, I.J. Hastings, A.J. Hains, Y. Kinoshita, "The Integrity of CNADU Fuel at Extended Burnups", Canadian Nuclear Society, Second International Conference on CANDU Fuel, Pembroke, Canada, 1989 October 1-5, pp 413-428.

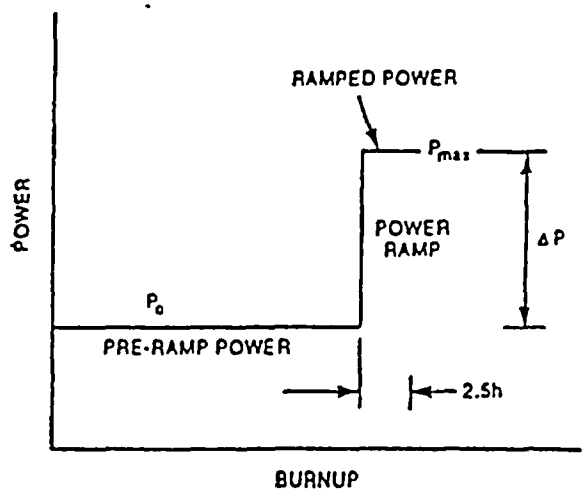

(a) POWER HISTORY

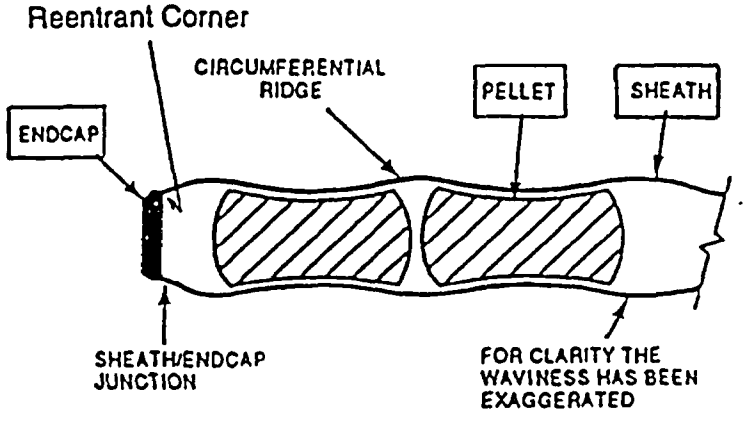

(b) FUEL ELEMENT

Figure 1: Definitions of Terms

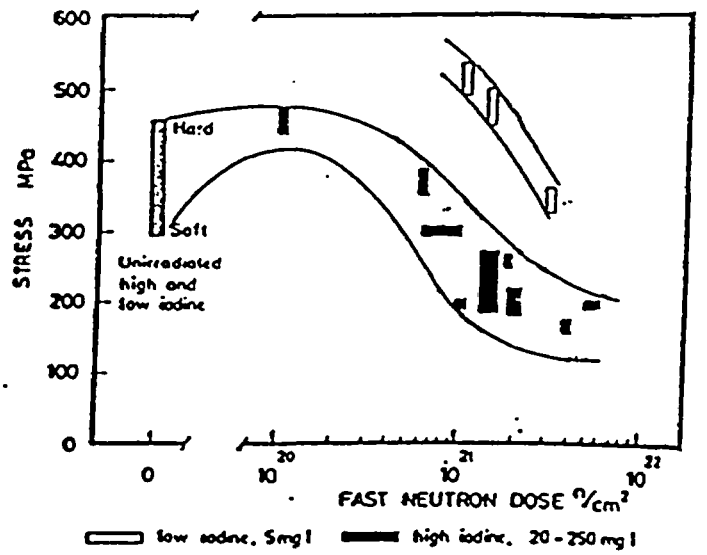

(a) Failure stress for SCC in 1-3 h.

(Reproduced from Lunde and Videm, 1980)

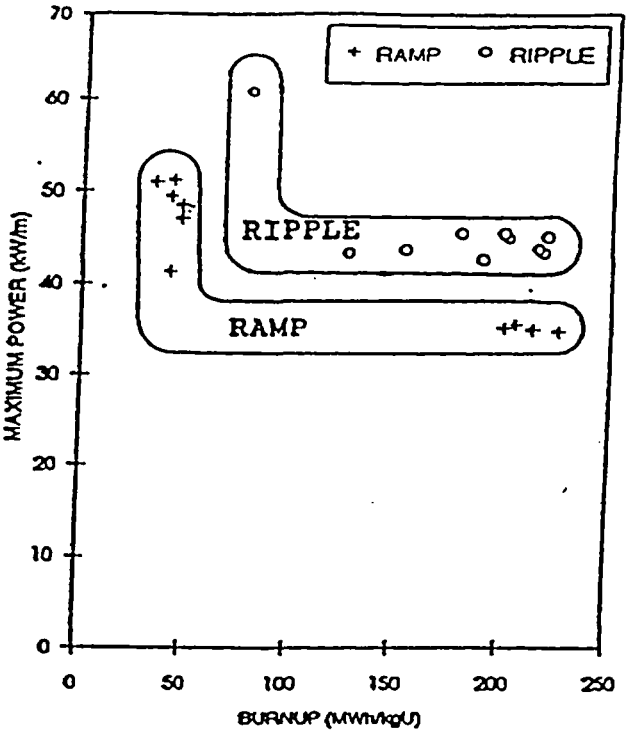

(b) Non-canlub defects near the maximum power thresholds

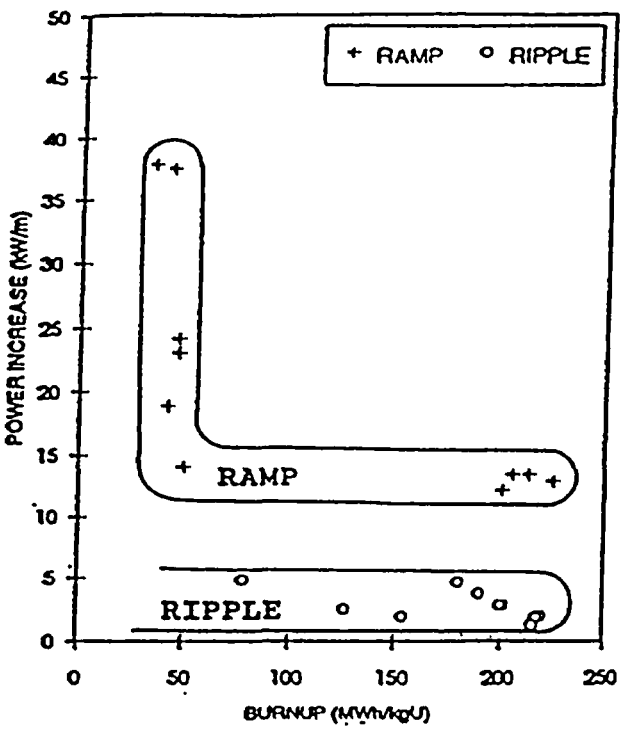

(c) Non-canlub defects near the power increase thresholds

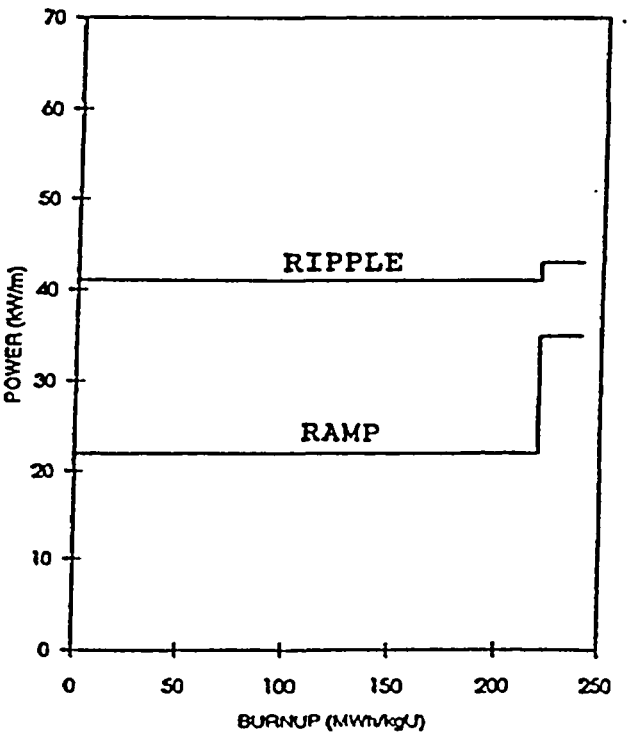

(d) Idealized power histories for ramps and ripples

Figure 2: Data for Failure Thresholds

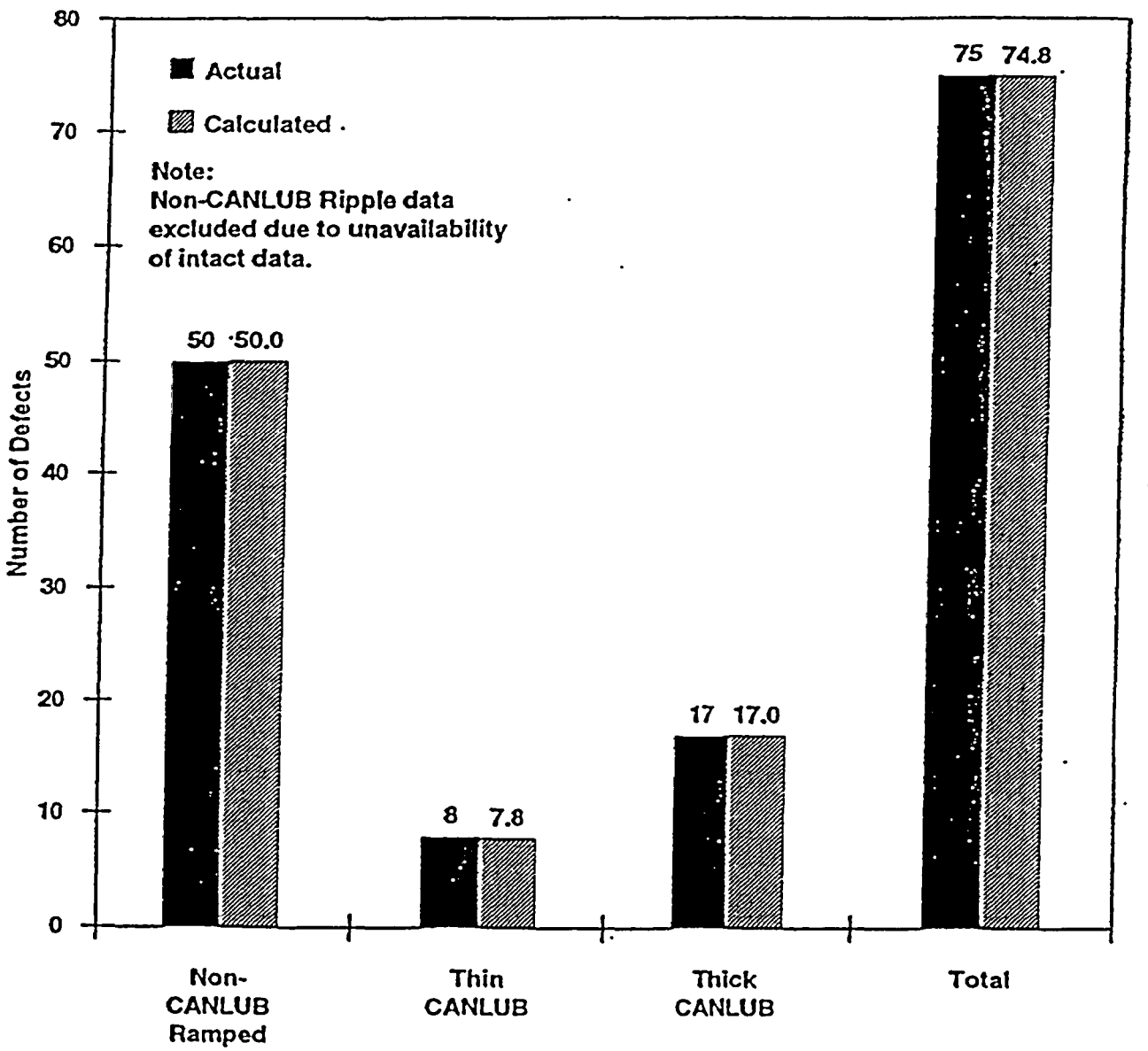

Figure 3: Number of Defects - Actual Versus Calculated

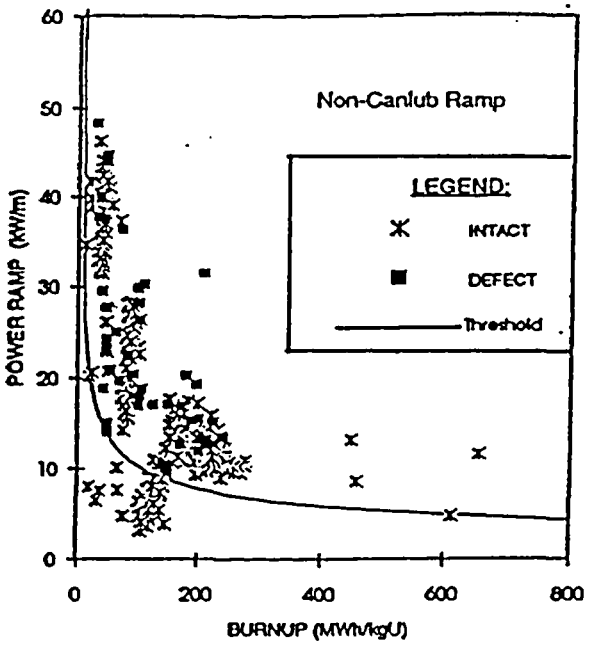

(a) Shape of the calculated non-canlub ramp defect threshold vs. data

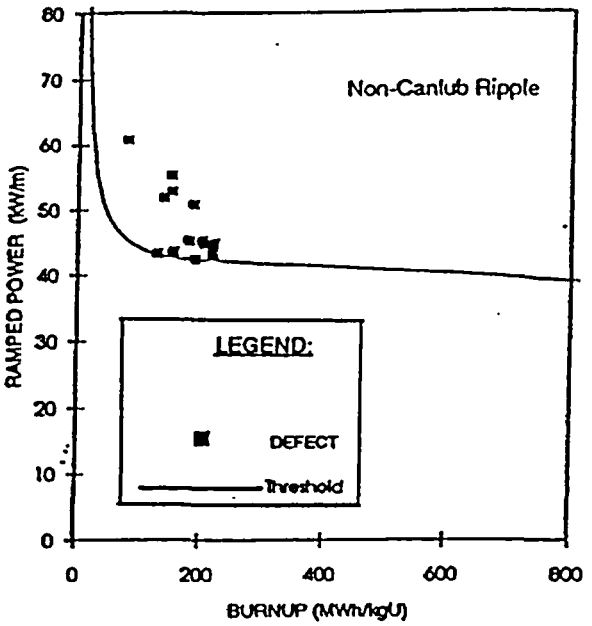

(b) Shape of the calculated non-canlub ripple defect threshold vs. data

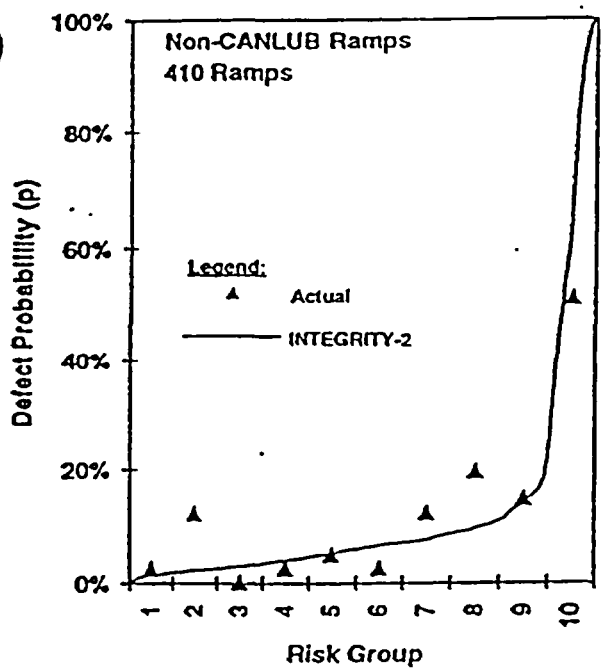

(c) Distribution of defects in risk groups

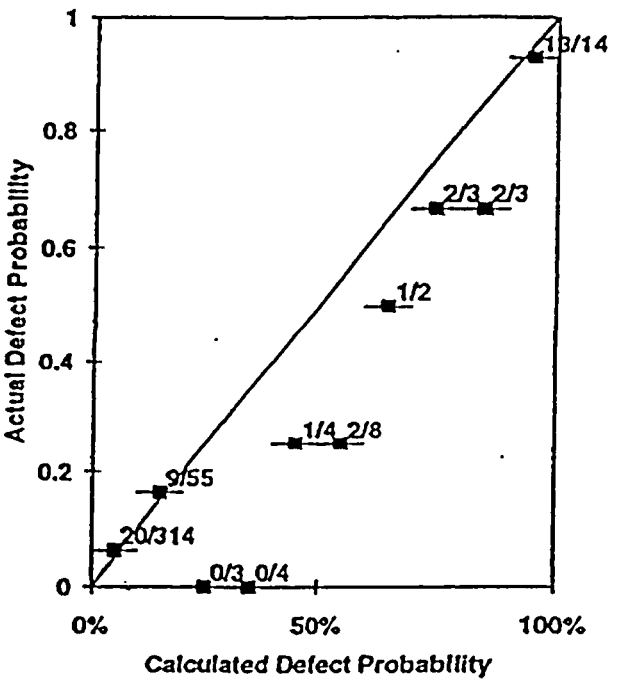

(d) Distribution of defects on the basis of defect probability

Figure 4: Distributions of Defects - Actual Versus Calculated

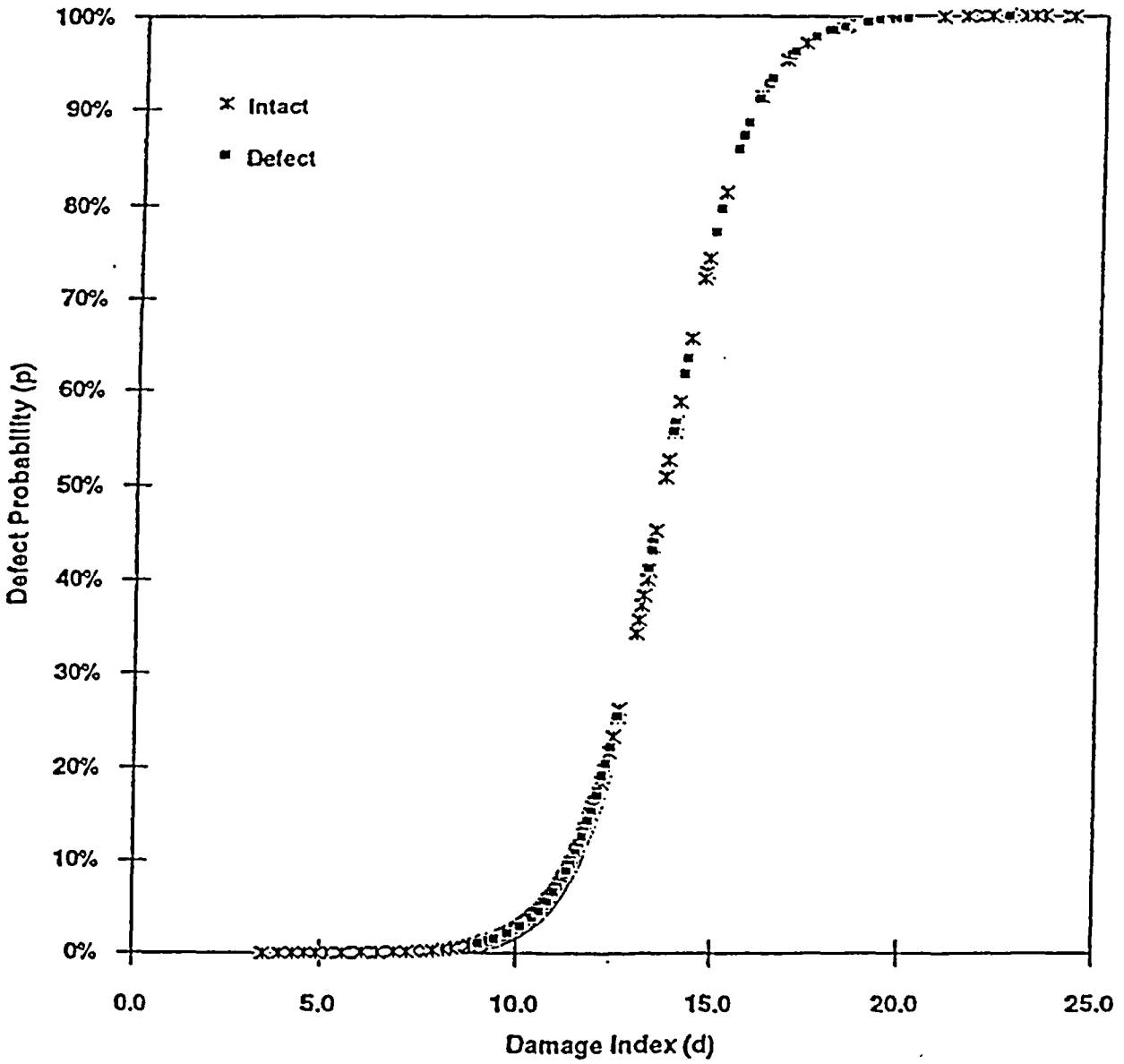

Figure 5: Defect Probability Versus Damage Index - All Data

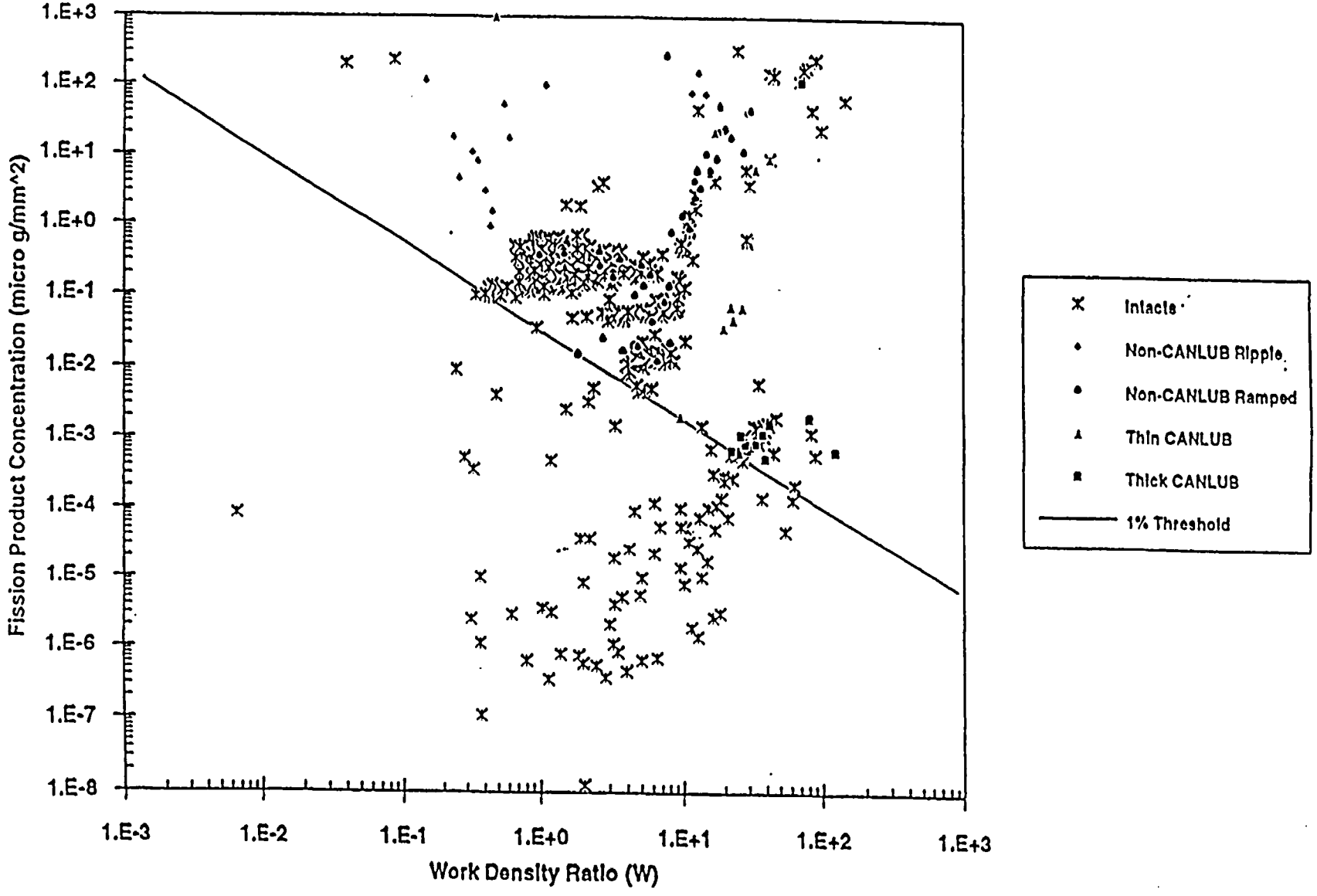

Figure 6: Defect Threshold for All Data

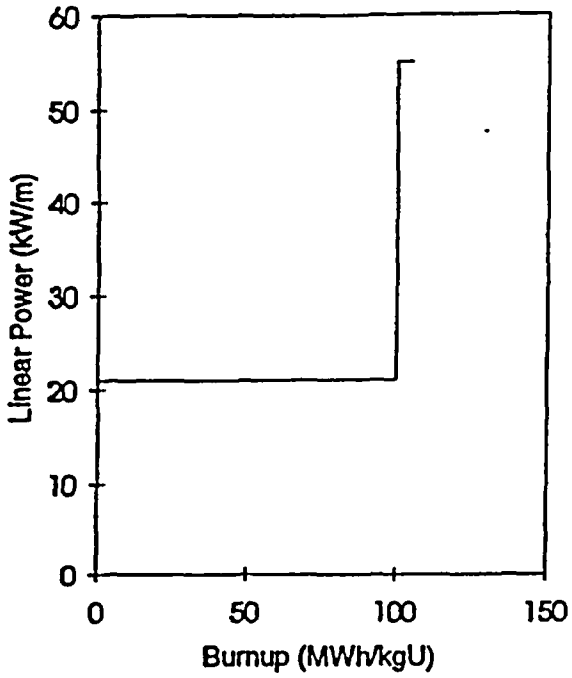

(a) Power Ramp Data
(Illustrative Example #1)

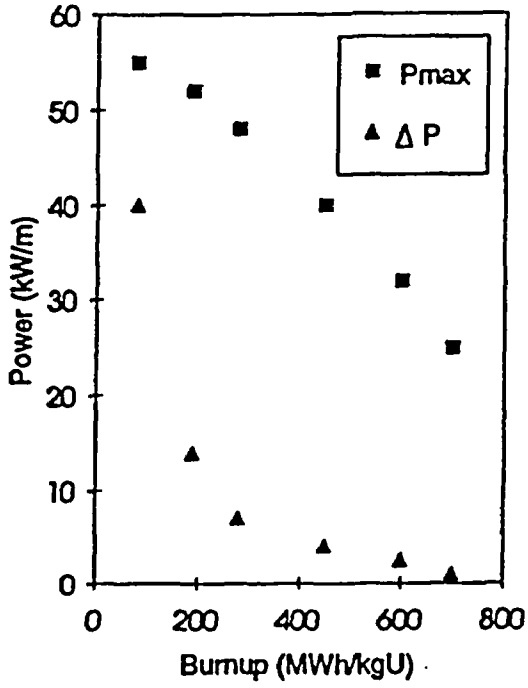

(c) Power History for
ALS CANDU Reactor
(Illustrative Example #2)

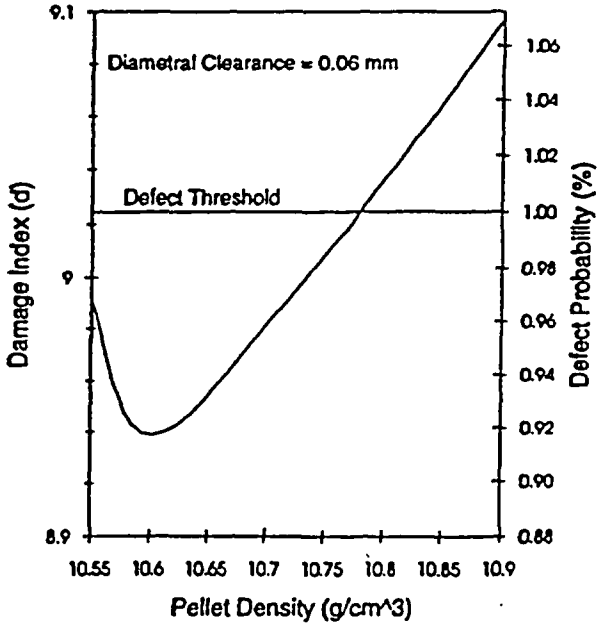

(b) Effect of Density
(Illustrative Example #1)

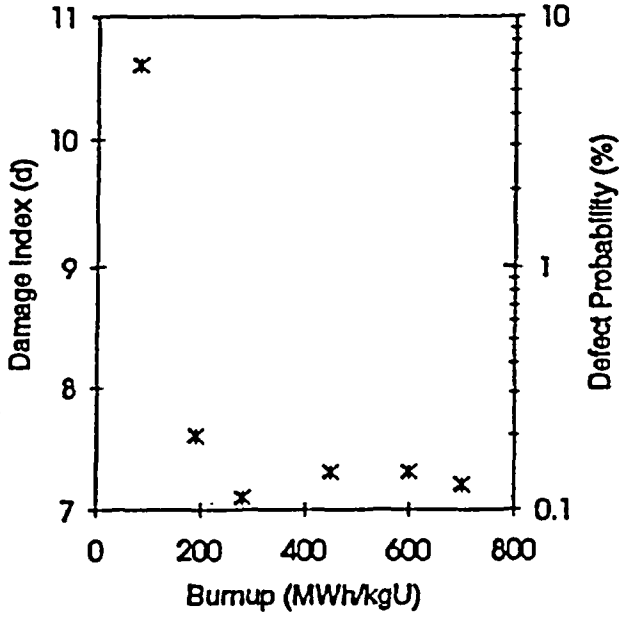

(d) Damage Index and
Defect Probability
(Illustrative Example #2)

Figure 7: Illustrative Examples